Catalysis Today 150 (2010) 207–212

Contents lists available at ScienceDirect

Catalysis Today

journal homepage: www.elsevier.com/locate/cattod

Study of the active phase of NiW hydrocracking sulfided catalysts obtained from an innovative heteropolyanion based preparation

Karima Ben Tayeb [a], Carole Lamonier [a,*], Christine Lancelot [a], Michel Fournier [a], Edmond Payen [a], Audrey Bonduelle [b], Fabrice Bertoncini [b]

[a] Unité de Catalyse et de Chimie du Solide, UMR CNRS 8181, Université des Sciences et Technologies de Lille, 59655 Villeneuve d'Ascq, France
[b] IFP-Lyon, Rond-point de l'échangeur de Solaize, BP-3, 69360 Solaize, France

ARTICLE INFO

Article history:
Available online 1 September 2009

Keywords:
Hydrocracking
NiWS
Heteropolytungstate
Silica–alumina

ABSTRACT

Hydrocracking (HCK) Nickel-Tungsten catalysts, supported on amorphous silica alumina, have been prepared by incipient wetness impregnation with new starting materials based on Keggin or on the derived lacunary Keggin heteropolyanion (HPA) structure and were compared to conventional catalysts. After calcination a polytungstate phase evidenced by Raman spectroscopy was generally observed indicating the destruction of the initial HPA. The sulfided solids were characterized by HRTEM to determine the dispersion of the WS_2 active phase. A careful XPS study indicated a better promoting effect for HPA based catalysts compared to their conventional counterparts. Toluene hydrogenation catalytic performances were related to the sulfided solids characterizations. $Ni_4SiW_{11}O_{39}$ nickel salt appeared to be the most efficient precursor that led to high dispersion and higher promoting effect due to the proximity of Ni and W in the heteropolyanion salt with an optimum Ni/W ratio.

1. Introduction

Developments of fuel market as well as specifications for more environmental-friendly products lead refiners to invest in processes for heavy oil conversion. Among them, hydrocracking (HCK) is a key process that produces selectively high quality middle distillate with low sulfur content. Hydrocracking catalysts are bifunctional, combining a hydro-dehydrogenating function with an acidic one. The hydro-dehydrogenation component is usually a mixed sulfide phase of groups VI and VIII metals. NiW couple is very attractive in hydrogenation of aromatic cycles and in hydrodenitrogenation reactions. Furthermore, the acidic function should be moderate in order to avoid cracking reactions which would yield gasoline instead of gas oil, as in the case of strongly acidic zeolite based catalysts [1]. Amorphous silica–aluminas (ASA) are known to present the appropriate acid strength [2]. For all these reasons, sulfided NiW/ASA catalysts are chosen in this study. The active phase consists of well dispersed WS_2 nanocrystallites decorated with Ni promoter atoms and is obtained by sulfiding an oxide precursor conventionally prepared by incipient wetness impregnation of an ASA support with an aqueous solution of ammonium metatungstate and nickel nitrate.

Based on previous work performed on CoMo catalyts [3,4], new methods of preparation of the oxidic precursors have been developed in our laboratory [5,6] in order to improve the catalytic performance of NiW/ASA sulfided catalysts. It consists of preparing new starting materials based on different heteropolytungstate nickel salts to improve promoting effect of nickel, via the increase of Ni/W ratio and via the proximity of Ni and W in the heteropolyanion salts themselves. This proximity of both elements has been considered by Van Veen et al. [7] as a criterion for obtaining good promoting effects by the Ni atoms. Moreover improved catalytic performances have been obtained for supported CoMo catalysts prepared with heteropolymolybdate cobalt salt [8].

In the present study, we first propose to use new starting materials based on Keggin or the derived lacunary Keggin heteropolyanion (HPA) structure, compared to conventional catalysts. After the preparation of the oxidic precursors and their characterization by Raman analysis, a detailed characterization of the active phase is given through the analysis performed by transmission electron microscopy and by X-ray photoelectron spectroscopy. Then, the catalytic performances of the different solids in toluene hydrogenation have been measured and correlated to the nature and the morphology of the active phase.

* Corresponding author. Tel.: +33 3 20 43 77 33; fax: +33 3 20 43 65 61.
E-mail address: carole.lamonier@univ-lille1.fr (C. Lamonier).

0920-5861/$ – see front matter © 2009 Elsevier B.V. All rights reserved.
doi:10.1016/j.cattod.2009.07.094

2. Experimental

2.1. Preparation of the impregnating solutions

Impregnating solutions were prepared according to two different routes:

(1) Conventional impregnating solutions were obtained by dissolution of ammonium metatungstate (AMT) and nickel nitrate in water, the Ni/W ratio varying between 0.125 and 0.36.
(2) Keggin-based solutions were prepared by dissolution in water of their corresponding nickel salts. Preparation and characterization of nickel salts $Ni_{3/2}PW_{12}O_{40}$, $Ni_2SiW_{12}O_{40}$, $Ni_4SiW_{11}O_{39}$ and $Ni_3PW_{11}NiO_{40}H$ have been already described [5,6]. In order to avoid the presence of counter ions (nitrate and ammonium present in conventional impregnating solutions) whose negative effect on hydrotreatment catalytic performances has been suggested [8], we have also prepared nickel salt of $H_2W_{12}O_{40}^{6-}$ metatungstate isopolyanion: this nickel salt was obtained in solution by cationic exchange in aqueous solution, of AMT and nickel perchlorate according to the following equation:

$$(NH_4)_6H_2W_{12}O_{40} + 3Ni(ClO_4)_2 \longrightarrow Ni_3H_2W_{12}O_{40} + \underline{6NH_4ClO_4}\downarrow$$

Ammonium perchlorate precipitate is then removed by filtration leading to the ($Ni_3H_2W_{12}O_{40}$) solution. The solid $Ni_3H_2W_{12}O_{40}$ is obtained by evaporation.

2.2. Preparation of the oxidic precursors

The oxidic precursors were prepared by incipient wetness impregnation of amorphous silica alumina (ASA) support [SiO_2(90)–Al_2O_3(10), specific area: 367 m^2/g, total pore volume: 0.7 ml/g] with previous impregnating solutions (1) and (2). After impregnation and 2 h of maturation in a wet atmosphere in order to let the species diffuse into the balls, the solids were dried overnight at 100 °C and then calcined at 500 °C under oxygen.

Table 1 lists the different nickel salts, the corresponding Ni/W ratios (checked by chemical analysis) and the nomenclature of new materials based catalysts. Reference catalysts with the same Ni/W ratio as those reported for the HPA nickel salts, have been prepared with conventional impregnating solutions. They were here after named RefA, RefB, RefC and RefDE in accordance to their corresponding Ni/W ratio. The quantity of WO_3 loading was chosen at 12 wt.% because it is the maximum loading obtained for the lowest soluble Keggin HPA nickel salt $Ni_{3/2}PW_{12}O_{40}$.

2.3. Preparation of the sulfided catalysts

The oxide precursors were sulfided in glass vial at atmospheric pressure under a H_2S/H_2 mixture with a $p(H_2S)/p(H_2)$ ratio about 0.17 and a gas flow of 2 L/(h g) of catalyst. The samples were heated under the sulfiding mixture at a rate of 5 °C/min up to 350 °C and maintained at this temperature for 2 h. They were then cooled down to 250 °C under the reactive mixture and then they were cooled down to room temperature under Argon to evacuate H_2S. Finally, Argon is evacuated and the glass vial is sealed to avoid any contact with air.

Table 1
Description of the catalysts prepared using the new starting materials or conventional impregnating solutions.

Catalysts nomenclature	Heteropolycompounds	Ni/W
A	$Ni_{3/2}PW_{12}O_{40}$	0.125
B	$Ni_2SiW_{12}O_{40}$	0.17
C	$Ni_3H_2W_{12}O_{40}$	0.25
D	$Ni_3PW_{11}NiO_{40}H$	0.36
E	$Ni_4SiW_{11}O_{39}$	0.36
RefA	$(NH_4)_6H_2W_{12}O_{40} + Ni(NO_3)_2$	0.125
RefB	$(NH_4)_6H_2W_{12}O_{40} + Ni(NO_3)_2$	0.17
RefC	$(NH_4)_6H_2W_{12}O_{40} + Ni(NO_3)_2$	0.25
RefDE	$(NH_4)_6H_2W_{12}O_{40} + Ni(NO_3)_2$	0.36

2.4. Liquid-phase toluene hydrogenation

Toluene hydrogenation is a model catalytic reaction to study HCK catalysts performances. In the mechanism of cracking, both acid and hydrogenating functions occur but balance between the number of hydrogenating sites and acid sites needs to be the biggest, explaining that the improvement of the hydrogenation function is wanted first. Indeed the catalysts were tested in toluene hydrogenation at high pressure to evaluate and to compare the hydrogenation function of each prepared catalyst. The test was conducted at 350 °C and 6 MPa. The liquid feed, which is also the feed used to sulfide, contained 73.6 wt.% cyclohexane, 20.0 wt.% toluene, 5.9 wt.% dimethyldisulfide, used as sulfiding agent and 0.5 wt.% aniline. Aniline was present to inhibit the acid function. The H_2/feed ratio was constant and equal to 450 Nl/L. The liquid feed flow was 16 $cm^3\ h^{-1}$ (LHSV of 4 h^{-1}) during the sulfidation stage and 8 $cm^3\ h^{-1}$ (LHSV of 2 h^{-1}) during the catalytic test. Catalysts balls were sieved and their diameter did not exceed 3 mm. This fraction was diluted in solid SiC (4 cm^3 for 4 cm^3 of catalyst). After sulfidation, conversion of toluene was determined by the analysis of effluent through on-line gas chromatography every 2 h after the first measurement. Catalytic results were expressed in terms of toluene hydrogenation (HYD) reaction rates, calculated from the measured toluene conversions (hydrogenation products).

2.5. Characterization techniques

2.5.1. XPS

XPS experiments were performed using a vacuum generator Escalab 220XI spectrometer. A monochromatized aluminium source was used for excitation. Binding energy (BE) values were referenced to the binding energy of C 1s (285 eV) and are given with an accuracy of ±0.1 eV. After their sulfidation under H_2/H_2S (85/15) for 2 h at 350 °C, samples were transferred in the spectrometer chamber using a gloves bag in order to avoid any reoxydation.

2.5.2. High resolution transmission electron microscopy (HRTEM)

High resolution transmission electron microscopy was performed on a TECNAI electron microscope operating at an accelerating voltage of 200 kV equipped with a LaB_6 filament. Freshly sulfided samples were ground under an inert atmosphere and dispersed in ethanol. The suspension was collected on carbon films supported on copper grids. For statistical analysis, length and stacking of 800 WS_2 slabs were determined for each sample.

2.5.3. Raman spectroscopy

The Raman spectra of the samples maintained at room temperature were recorded using a Raman microprobe equipped with a photodiode array detector. The exciting laser source was the 532 nm line of a Nd-YAG laser. The wavenumber accuracy was 2 cm^{-1}.

3. Results

3.1. Characterization by Raman spectroscopy of calcined oxidic precursors

In a previous study [5,6], we showed by Raman spectroscopy that the spectra of calcined oxidic precursors based on conven-

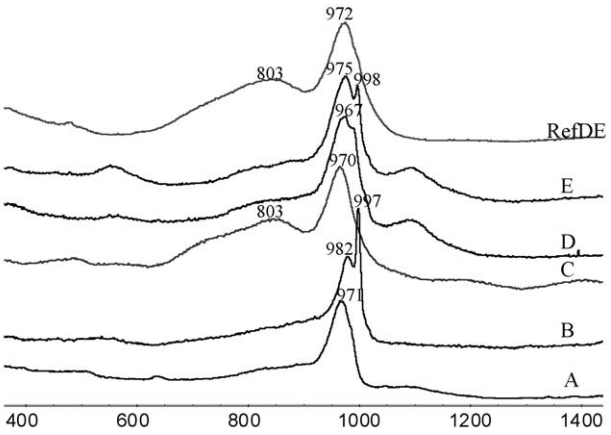

Fig. 1. Raman spectra of ASA supported oxidic precursors for A, B, C, D, E and RefDE solids.

tional precursors exhibit a main line at 970 cm^{-1} which is characteristic of the presence of well dispersed polytungstate species. As observed in Fig. 1, similar features are observed for the HPA oxidic precursors containing phosphorus species (solids A and D) and the $Ni_3H_2W_{12}O_{40}$ based solids, indicating that in this case the HPA phase is not preserved after calcination. A different behavior is observed for the $Ni_4SiW_{11}O_{39}$ and $Ni_2SiW_{12}O_{40}$ based solids. The Raman spectrum of $Ni_2SiW_{12}O_{40}$ calcined catalyst (Fig. 1B) corresponds to the $SiW_{12}O_{40}^{4-}$ HPA features. This indicates that the $SiW_{12}O_{40}^{4-}$ entities could be destroyed during calcination at 500 °C and then could be re-formed after thermal treatment and transfer in air. The decomposition of this HPA on the calcined solid is suggested by thermal analysis of bulk $Ni_2SiW_{12}O_{40}$ HPA salt (not presented here) showing the latest weight loss around 400 °C and the formation of crystallized WO_3 at 600 °C with the apparition of an endothermic peak in the differential thermogravimetric analysis curve. Nevertheless the behavior of supported HPA could be different and the hypothesis of HPA preservation on the support has to be kept in mind.

For $Ni_4SiW_{11}O_{39}$ based catalyst, Raman analysis (Fig. 1E) shows a line at 975 cm^{-1} that is assigned to a polytungstate phase whereas the narrow line at 998 cm^{-1} should arise from the formation of $SiW_{12}O_{40}^{4-}$ species. These latter entities should also come from support dissolution after thermal treatment and transfer in air.

3.2. Characterization of the sulfided catalysts

3.2.1. XPS characterizations

Fig. 2A shows W 4f XPS spectra of D, E and RefDE catalysts after sulfidation in a H_2S/H_2 mixture at 350 °C for 2 h. Whatever the solid, a doublet with the $4f_{7/2}$ peak at 32.8 eV is observed. This XPS photopeak is assigned to W-sulfide with an oxidation state of 4+ as reported in the literature [9]. The W 4f photopeak is almost similar for all the catalysts which have been calcined and sulfided in the same conditions. Indeed, Van Der Meer et al. [10] showed that calcination and sulfidation temperatures have a pronounced effect on the sulfidation degree. The W 4f XPS photopeak mainly shows that the sulfidation at 350 °C allows to obtain a large proportion of WS_2 phase for all catalysts. The Ni 2p spectra (Fig. 2B) of D, E and RefDE sulfided catalysts exhibit a Ni 2p peak at about 853.6 eV characteristic of Ni in a sulfur environment [11].

A systematic decomposition of the XPS W 4f and Ni 2p peaks was performed for all the catalysts. Fig. 3A and B presents typical decomposition obtained on a conventional catalyst and is representative of decomposition performed on all sulfided catalysts. The decomposition of the W 4f (Fig. 3A) photopic shows

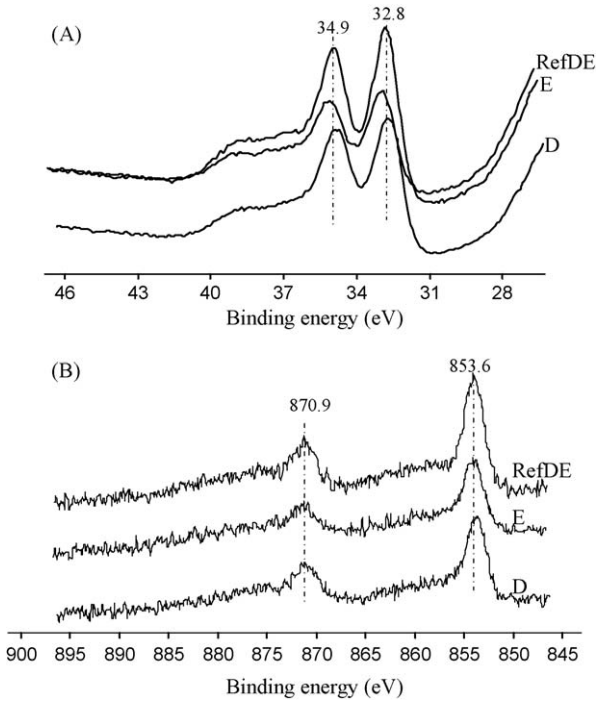

Fig. 2. XPS spectra. (A) W 4f spectra: D, E, and RefDE. (B) Ni 2p spectra: D, E, and RefDE.

three contributions attributed to W 6+ in an oxidic environment generally proposed as a WO_3 phase (W $4f_{7/2}$: 36 eV, W $4f_{5/2}$: 38.1 eV), oxysulfide WOxSy (W $4f_{7/2}$: 33.5 eV, W $4f_{5/2}$: 35.5 eV) and sulfidic WS_2 entities (W $4f_{7/2}$: 32.2 eV, W $4f_{5/2}$: 34.3 eV). For Ni, three

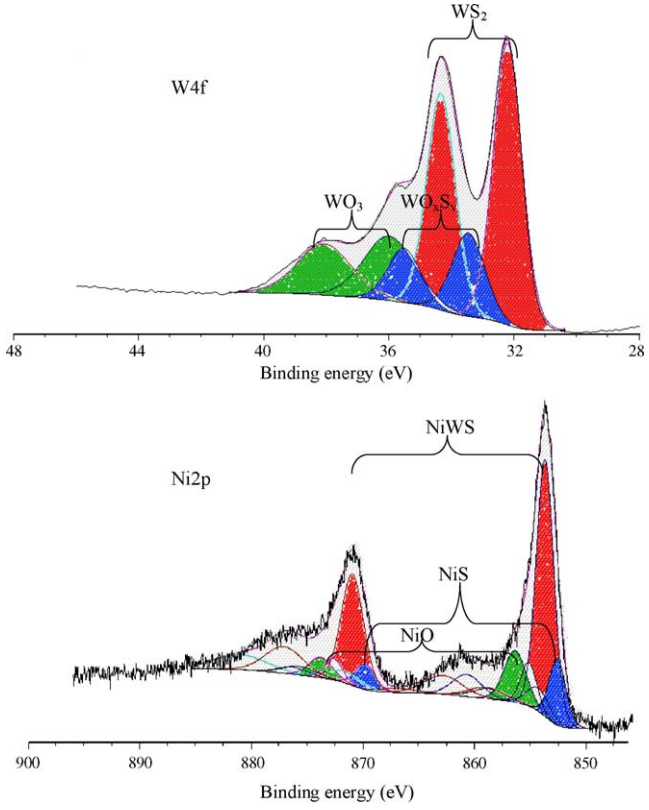

Fig. 3. Example of decomposition of XPS spectra after sulfidation at 350 °C. (A) W 4f spectrum: contribution of $W^{IV}S_2$ phase, Contribution of W^{V} oxysulfide phase and contribution of W^{VI} oxidic phase. (B) Ni 2p spectrum: contribution of NiWS phase, contribution of NiS and contribution of oxidic phase.

Table 2
XPS data of the various catalysts sulfided under gas phase at 350 °C.

Catalysts nomenclature	WS_2 quantity[a] (%)	NiWS quantity[b] (%)	Sulfide quantity[c] (%)
A	50	50	92
RefA	52	42	92
B	61	60	90
RefB	56	53	93
C	59	49	94
RefC	57	43	93
D	58	50	93
E	50	52	91
RefDE	55	48	92

[a] Obtained from the decomposition of W 4f photopeak.
[b] Obtained from the decomposition of Ni 2p photopeak.
[c] Obtained from the decomposition of S 2p photopeak.

contributions are exhibited (Fig. 3B), two sulfidic NiS (Ni $2p_{3/2}$: 852.6 eV, Ni $2p_{1/2}$: 869.8 eV), NiWS (Ni $2p_{3/2}$: 853.7 eV, Ni $2p_{1/2}$: 870.9 eV) and an oxidic phase (Ni $2p_{3/2}$: 856.4 eV, Ni $2p_{1/2}$: 873.8 eV). These bending energies values corresponding to the three contributions (NiS, NiWS and Ni in an oxidic phase) of the Ni $2p_{3/2}$ photopeak are in agreement with those reported in the literature [12,13] for supported NiW sulfided catalysts. Ni $2p_{1/2}$ photopeak contributions are attributed considering a spin orbit of 17.2 ± 0.2 eV. Contributions colored in white (Fig. 3B) are the corresponding satellite peaks of the principal ones. The decomposition of S 2p photopeaks (not presented here) evidenced two contributions assigned to sulfide (161.8 eV) and oxysulfide entities (163 eV).

Careful decomposition allows to estimate the sulfidation degree of tungsten (expressed as WS_2% of the total W) as well as the global sulfidation degree expressed as the quantity of sulfide species in the global amount of sulfur.

The values reported in Table 2 indicate little variation of the quantity of sulfided W between both series of catalysts. For reference compounds this value varies between 52% and 57% whereas for HPA based catalysts, it varies between 50% and 61%. Nevertheless, as reported in literature [14], the sulfidation of tungsten is not complete even at 600 °C. Van Der Meer et al. [10] reported that at 400 °C, only 50% of tungsten is in an oxidation state of 4+, which is in agreement with our results.

Through careful decomposition, the amounts of NiO, NiS and NiWS phase have been determined and the corresponding quantity of NiWS phase (expressed as NiWS% of the total Ni) are reported in Table 2, between 42% and 60%. Hensen et al. [15] show that 48% of NiWS sulfidation degree is obtained for a calcination and sulfidation temperature of 400 °C. We can also notice that the quantity of NiWS phase in the case of heteropolyanion based catalysts is always larger than in the case of conventional precursors.

Moreover, the decomposition of S 2p spectra (not shown here) indicates that sulfur species are mainly present as sulfide (90–94%), this quantity being almost constant whatever the precursor used, as reported in Table 2.

Decomposition results have been expressed as (NiWS)/(WS_2) XPS ratio as a function of (Ni/W) ratio as reported in Fig. 4 for reference and HPA based catalysts. The quantity of NiWS phase is more important when the ratio Ni/W becomes more significant.

Though the global sulfidation is almost the same for all catalysts, a better promoting effect of nickel is observed with catalysts based on heteropolyanion compared to conventional precursor. This better promoting effect is largely higher in the case of E catalyst.

3.2.2. HRTEM

Five catalysts have been studied by HRTEM, corresponding to Ni/W ratio of 0.125 and 0.36 (A, D, E) and their corresponding reference catalysts (RefA and RefDE).

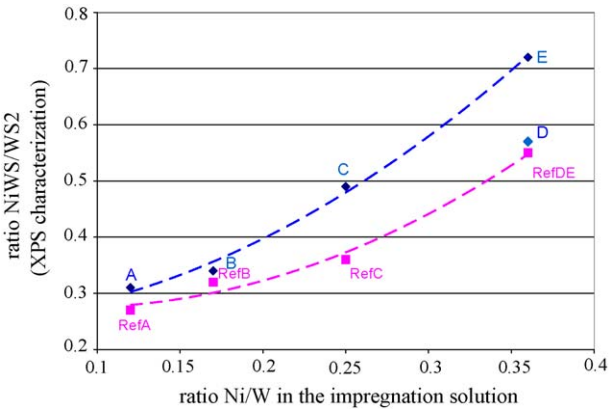

Fig. 4. Promoting effect of nickel calculated from XPS data.

The morphology of the WS_2 slabs was characterized by HRTEM. Typical images are given in Fig. 5 for sulfided catalyst E (Fig. 5A) and his sulfided reference catalyst RefDE (Fig. 5B). The presence of WS_2 slabs is clearly visible for each catalyst with the typical layered structure of WS_2. The observation of various photos shows a heterogeneous distribution of the slabs over the ASA support, with areas showing very few or no slabs areas with a majority of single WS_2 slabs, while areas densely populated with multiple-stacked slabs were also found. Van der Meer et al. [10] demonstrated by EDX analysis that the WS_2 slabs are preferentially

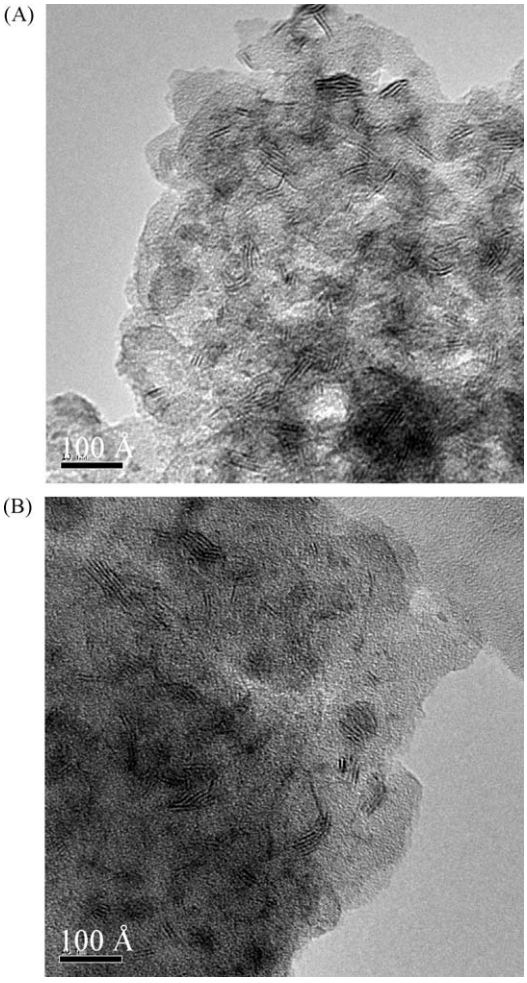

Fig. 5. Typical HREM micrographs of (A) sulfided E and (B) sulfided RefDE.

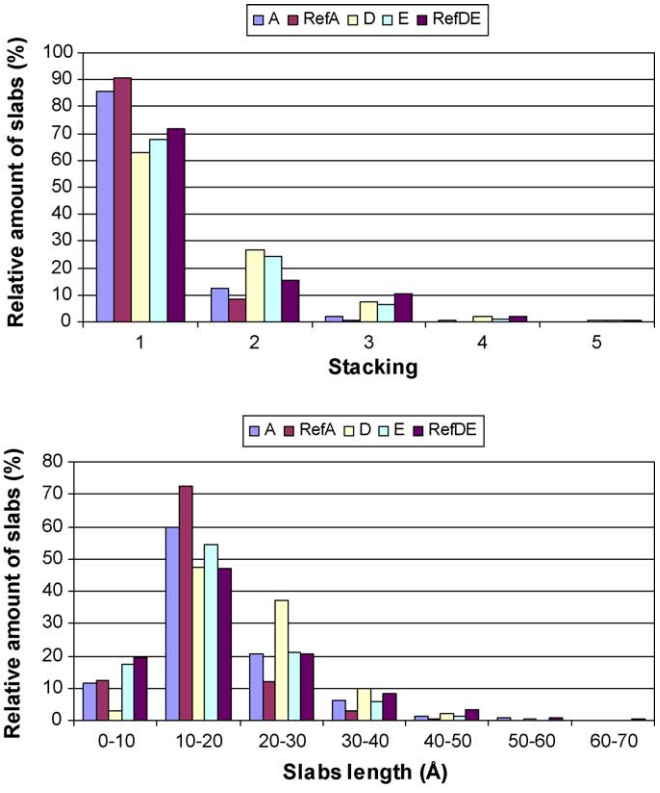

Fig. 6. Distribution of length and stacking of the WS_2 slabs of the various catalysts after sulfidation under gas phase at 350 °C for 2 h.

located on the alumina part of the ASA support, indicating that tungsten preferentially interacts with the alumina part of the support materials. In our case, the ASA support consists mainly of silica (10% alumina, 90% silica), the heterogeneity of the slabs distribution may be more probably attributed to the poor dispersion usually observed on silicic materials.

The distribution of the length and stacking degree of WS_2 slabs for A, RefA, D, E and RefDE catalysts are reported in Fig. 6 and the average slab length and stacking degree of catalysts are listed in Table 3.

For all catalysts, the slab length distribution is centred on the [10–20] Å interval giving corresponding average values in the range of 15–21 Å. These values are smaller than those reported in the literature. However the WS_2 active phase was dispersed on different supports such as alumina, carbon, or different ASA materials with different sulfidation conditions [10–15–16]. Hensen et al. [15] have determined an average slab length of 33 Å on catalysts sulfided at 400 °C supported on carbon and alumina, presenting a Ni/W ratio of 0.25. For Vissenberg et al. [16], the slab length is centred on the [20–40] Å interval for NiW/Al_2O_3 catalysts sulfided at 400 °C and 650 °C with a sulfidation pressure of respectively 15 and 1 bars (Ni/W ratio of 0.25). Van der Meer et al. [10] studied a NiW catalyst (Ni/W ratio of 0.25) supported on ASA material (60% alumina, 40% silica) sulfided at 400 °C under

Table 3
Average slab length, average stacking of studied catalysts.

Catalysts nomenclature	Average slab length (Å)	Average stacking degree
A	17	1.2
RefA	15	1.2
D	21	1.5
E	17	1.5
RefDE	18	1.5

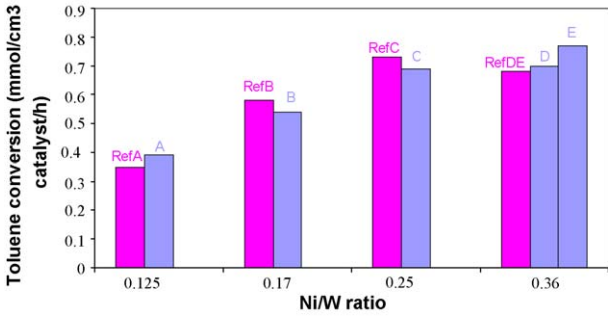

Fig. 7. Hydrogenation activity of catalysts prepared with conventional impregnating solutions and HPA nickel salts.

atmospheric pressure and reported an average slab length of 29 Å. Irrespective of the support and the sulfidation conditions, the results found in the literature give much larger average length of the WS_2 slabs than those calculated for our catalysts supported on ASA material with an alumina–silica ratio of 10/90, with Ni/W ratio varying between 0.125 and 0.36. Concerning the slabs stacking, single-layered slabs are predominant as reported in the literature [15,16].

In Table 3, one can notice that for a same Ni/W ratio, the average stacking is identical for the HPA based catalysts and their conventional counterpart. The average lengths of the HPA based catalysts were found of the same magnitude than those obtained for the conventional ones, except for the D catalyst, which presents a larger average length of 21 Å.

3.2.3. Catalytic results: toluene hydrogenation

Catalytic performance versus the nature of the starting materials and the Ni/W ratio are reported in Fig. 7, the W loading being fixed at 12 wt.% WO_3. As observed for conventional catalysts, the activity of HPA based catalysts increased when the Ni/W ratio was raised [4]. The optimum value is known to vary with the considered support, more or less Ni species being available for promotion, depending on the interactions observed between the support and the deposited surface species. Vissenberg et al. [16] found that the optimum Ni/W ratio for NiW/TiO_2 (0.4) was lower than that for NiW/Al_2O_3 (0.6). On our catalysts, the ratios equal to 0.25 and 0.36 resulted in higher activities than those of the smaller ones (0.125 and 0.17).

The A, B, C and D catalysts presented catalytic performance equivalent to those of their reference catalysts, whereas catalyst E prepared with $Ni_4SiW_{11}O_{39}$ appeared as more hydrogenating than its reference catalyst. As $Ni_4SiW_{11}O_{39}$ salt is sufficiently soluble in water to prepare solids with a higher WO_3 loading than 12 wt.%, we have then prepared a $Ni_4SiW_{11}O_{39}$ based catalyst and its reference with 17 wt.% WO_3 loading. Results (Fig. 8) show clearly that the

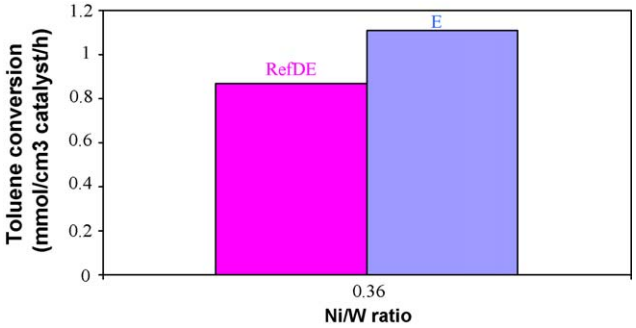

Fig. 8. Hydrogenation activity of catalysts prepared with 17 wt.% WO_3 loading.

$Ni_4SiW_{11}O_{39}$ based catalyst is 30% more hydrogenating than its counterpart prepared with conventional precursors, confirming the trend previously evidenced on this catalyst with a 12 wt.% WO_3 loading.

4. Discussion

Several catalysts have been prepared with a Ni/W ratio varying between 0.125 and 0.36. The corresponding activity in toluene hydrogenation increases with the Ni/W ratio, the optimum value being observed between 0.25 and 0.36.

For catalysts A based on $Ni_{3/2}PW_{12}O_{40}$ and RefA exhibiting the lowest Ni/W ratio, XPS studies point out a low sulfidation degree of tungsten (respectively 50% and 52% of W phase) together with a low promoting effect with a very close value for the two solids. These results explain the similar and poor catalytic performances of A and RefA.

The observation of the Raman spectra shows, for all the catalysts after calcination, the presence of well dispersed polytungstate phase, except for catalyst B based on $Ni_2SiW_{12}O_{40}$ for which the features of the HPA are present after calcination. A low promoting effect is also observed for this catalyst that could be induced by the presence of the HPA after calcination.

A better promoting effect is observed for the catalyst C based on $Ni_3H_2W_{12}O_{40}$ compared to its conventional counterpart RefC. However, the C catalyst exhibits a catalytic performance similar to its reference, in any case lower than what we could expect from its high promoting effect. A poor dispersion in catalyst C could explain this observation and complementary characterizations are currently under progress for a better understanding of this point.

Catalytic activity of solid D based on $Ni_3PW_{11}NiO_{40}H$ is almost the same than its reference catalyst, in agreement with similar promotion degree. It however exhibits a much lower performance than catalyst E, prepared from the $Ni_4SiW_{11}O_{39}$ HPA and having the same Ni/W ratio. Let us note that in the $Ni_3PW_{11}NiO_{40}H$ HPA, one Ni atom is in the Keggin structure, which could be detrimental to further availability of Ni for promotion. The average slab length on catalyst D is slightly higher than catalyst E and RefDE but a careful observation of the length distribution shows for this solid a singular behavior with 3% of slabs under 10 Å (18% for solid E and 20% for RefDE), 48% of slabs between 10 and 20 Å (55% for solid E and 48% for RefDE), 38% of slabs between 20 and 30 Å (20% for solid E and for RefDE). The low performance of catalyst D can then be related to a poor dispersion of the active phase together with a low promoting effect of Ni. The catalyst E based on $Ni_4SiW_{11}O_{39}$ reveals a similar slab length and stacking degree than its reference RefDE. However, a better promoting effect is observed on E than on RefDE catalyst, in agreement with the better catalytic performance observed for catalyst E. This result evidenced the beneficial and promising effect of the $Ni_4SiW_{11}O_{39}$ heteropolyanion as a precursor for hydrogenation catalysts.

For all catalysts, it appears that the use of HPA enhances the promoting effect. More over this promoting effect increases with the Ni/W ratio, indicating that the Ni atoms added through the HPA structure are directly available for promotion of the WS_2 phase.

5. Conclusions

In this work, well-defined HPA, associating W and Ni in the same entity, which has been characterized in a previous work [6], has been deposited by incipient wetness impregnation on an amorphous silica–alumina support to prepare HCK oxidic precursors. A comparison between two preparation methods of NiW catalysts has been undertaken through impregnation with solutions containing AMT and nickel nitrate or the heteropolyanions with a Ni/W ratio varying between 0.125 and 0.36. Toluene hydrogenation conversions showed that the best catalytic result was obtained for the catalyst based on $Ni_4SiW_{11}O_{39}$ precursor. This HPA where W and Ni are inserted in the same entity with an optimum Ni/W ratio permitted to have the best promoting effect by the nickel atoms. Moreover, a good dispersion was also obtained for this HPA. Both results explained the catalytic performance obtained in toluene hydrogenation, in relation with an optimization of the active phase.

Acknowledgements

We are thankful to our colleagues from IFP for their help: N. Lett, Y. Mertz, P. Lecour and C. Legens.

References

[1] I.E. Maxwell, Catal. Today 1 (1987) 385.
[2] A. Corma, A. Martinez, V. Martinez-Soria, J.B. Monton, J. Catal. 153 (1995) 25.
[3] C. Martin, C. Lamonier, M. Fournier, O. Mentré, V. Harlé, D. Guillaume, E. Payen, Chem. Mater. 17 (2005) 4438.
[4] C. Lamonier, C. Martin, J. Mazurelle, V. Harlé, D. Guillaume, E. Payen, Appl. Catal. B: Environ. 70 (2007) 548.
[5] K. Ben Tayeb, C. Lamonier, M. Fournier, E. Payen, F. Bertoncini, A. Bonduelle, Am. Chem. Soc. Div. Fuel Chem. 53 (2008) 9.
[6] K. Ben Tayeb, C. Lamonier, C. Lancelot, M. Fournier, E. Payen, F. Bertoncini, A. Bonduelle, Comptes Rendus de Chim. 12 (2009) 692.
[7] J.A.R. Van Veen, P.A.J.M. Hendriks, R.R. Andrea, E.J.G.M. Romers, A.E. Wilson, J. Phys. Chem. 94 (1990) 5282.
[8] J. Mazurelle, C. Lamonier, C. Lancelot, E. Payen, C. Pichon, D. Guillaume, Catal. Today 130 (2008) 41.
[9] H.R. Reinhoudt, E. Crezee, A.D. Van Langeveld, P.J. Kooyman, J.A.R. Van Veen, J.A. Moulijn, J. Catal. 196 (2000) 315.
[10] Y. Van Der Meer, E.J.M. Hensen, J.A.R. Van Veen, A.M. Van Der Kraan, J. Catal. 228 (2004) 433.
[11] G. Kishan, L. Coulier, V.H.J. De Beer, J.A.R. Van Veen, J.W. Niemantsverdriet, J. Catal. 196 (2000) 180.
[12] B. Guichard, M. Roy-Auberger, E. Devers, C. Legens, P. Raybaud, Catal. Today 130 (2008) 97.
[13] D. Eliche-Quesada, J. Mérida-Robles, P. Maireles-Torres, E. Rodrıguez-Castellón, A. Jiménez-López, Appl. Catal. A: Gen. 262 (2004) 111.
[14] P.J. Mangnus, A. Bos, J.A. Moulijn, J. Catal. 146 (1994) 437.
[15] E.J.M. Hensen, Y. Van Der Meer, J.A.R. Van Veen, J.W. Niemantsverdriet, Appl. Catal. A: Gen. 322 (2007) 16.
[16] M.J. Vissenberg, Y. Van Der Meer, E.J.M. Hensen, V.H.J. De Beer, A.M. Van Der Kraan, R.A. Van Santen, J.A.R. Van Veen, J. Catal. 198 (2001) 151.